Cell. Mol. Life Sci. (2011) 68:661–676
DOI 10.1007/s00018-010-0472-x

Cellular and Molecular Life Sciences

RESEARCH ARTICLE

Efficiency of nonhomologous DNA end joining varies among somatic tissues, despite similarity in mechanism

Sheetal Sharma · Bibha Choudhary · Sathees C. Raghavan

Received: 12 May 2010 / Revised: 7 July 2010 / Accepted: 16 July 2010 / Published online: 3 August 2010
© Springer Basel AG 2010

Abstract Failure to repair DNA double-strand breaks (DSBs) can lead to cell death or cancer. Although nonhomologous end joining (NHEJ) has been studied extensively in mammals, little is known about it in primary tissues. Using oligomeric DNA mimicking endogenous DSBs, NHEJ in cell-free extracts of rat tissues were studied. Results show that efficiency of NHEJ is highest in lungs compared to other somatic tissues. DSBs with compatible and blunt ends joined without modifications, while non-compatible ends joined with minimal alterations in lungs and testes. Thymus exhibited elevated joining, followed by brain and spleen, which could be correlated with NHEJ gene expression. However, NHEJ efficiency was poor in terminally differentiated organs like heart, kidney and liver. Strikingly, NHEJ junctions from these tissues also showed extensive deletions and insertions. Hence, for the first time, we show that despite mode of joining being generally comparable, efficiency of NHEJ varies among primary tissues of mammals.

Keywords DNA double-strand break · DSB repair · NHEJ · DNA damage · Genomic instability · Lung cancer · Heart

Electronic supplementary material The online version of this article (doi:10.1007/s00018-010-0472-x) contains supplementary material, which is available to authorized users.

S. Sharma · B. Choudhary · S. C. Raghavan (✉)
Department of Biochemistry, Indian Institute of Science, Bangalore 560 012, India
e-mail: sathees@biochem.iisc.ernet.in

B. Choudhary
Manipal Institute of Regenerative Medicine, Manipal University, Bangalore 560 071, India

Abbreviations

NHEJ	Nonhomologous end joining
DSB	Double-strand break
HR	Homologous recombination
PSL U	Photo stimulated luminescence unit
BSA	Bovine serum albumin
DAPI	4,6-Diamidino-2-phenylindole
PCR	Polymerase chain reaction
IP	Immunoprecipitation
RT-PCR	Reverse transcriptase PCR

Introduction

Maintenance of genomic integrity and stability is of prime importance for the survival of an organism, as the DNA is consistently exposed to various types of lesions. DNA double-strand breaks (DSBs) are considered as the most deleterious type of damage, as failure of their repair could lead to chromosomal translocations and cancer or cell death [1–4]. DSBs can be generated exogenously by ionizing radiation and chemotherapeutic agents like bleomycin or endogenously by free radicals, replication across a nick and physiological processes such as V(D)J recombination, class switch recombination, meiosis, etc. [5, 6]. Approximately, 10–100 endogenous DSBs are generated per nucleus per day [7]. DSBs can be repaired by two major pathways in mammalian cells, namely homologous recombination (HR) and nonhomologous end joining (NHEJ) [8–10]. HR requires a region of extensive homology, operates during late S and G2 phases of the cell cycle, and is accurate. On the other hand, NHEJ does not require a region of homology and operates in all phases of cell cycle but is error prone [11–13]. However, such errors introduced

during NHEJ pose little threat to the genome as only a small percentage of these errors exist in regions encoding for protein, whereas entering into S or G2 phase with unrepaired DNA is a major risk.

The key players of NHEJ are a set of proteins which recognize the broken DNA molecules and process the ends to make them ligatable [8, 10, 14–16]. Firstly, the broken DNA ends are recognised by KU70/KU80 heterodimer, which recruit DNA-PKcs in association with ARTEMIS [17–19]. The DNA ends are processed by either ARTEMIS or DNA-PKcs-ARTEMIS complex to create ligatable ends [20, 21]. After processing, the ends are filled using POL X family members, POLμ (fill-in synthesis of 3′ overhangs) and POLλ (fill-in synthesis of 5′ overhangs) [22–24]. Finally, the ends are ligated by XLF:XRCC4:DNA LIGASE IV complex [25–27].

Studies thus far to understand the mechanism of NHEJ were performed mostly on cell lines by using plasmid DNA substrates containing DSBs in a cell-free system or by transfection [28–34]. These cell lines have been derived from specific cell types like B cells (GM00558), cervical cancer epithelial cells (HeLa), lung alveolar basal epithelial cells (A549), human acute lymphocytic leukemic cells (HPB-ALL), glioblastoma cells (M059K), etc. [35–37]. Most of these studies were in isolation and hence do not compare efficiencies between different cell types. Moreover, since the cell lines were derived from a particular cell type and grown in vitro, the repair efficiency of one cell may not reflect that of the entire organ from which it was generated.

Cell lines divide actively whereas most of the cells in a tissue are in resting phase, G_0 [38]. Glioma cell lines have been shown to possess a less efficient DNA repair capacity as compared to normal human astrocytes [39]. Lower repair efficiency has also been reported in L1210 cell line, compared to the in vivo ascitic fluid culture [40]. Besides, it has been reported that expression profile of most of the cell lines is different from that of tissues of their origin [41]. Moreover, since most of the cell lines are derived from tumor tissues, their origin itself is controversial at times, as most of the cancers are metastatic [42].

Recently, one of the studies used mouse testicular cell-free system to understand NHEJ in germ cells [43, 44]. Similar attempts were made to study NHEJ in rat neurons [45, 46]. Surprisingly, there are no studies in the literature that compare the efficiency and mechanism of NHEJ in somatic tissues of different organs in mammals. Since organs consist of multiple types of cells, it would represent the physiological state better. Hence, the current study is focused on unravelling the mechanistic differences of NHEJ among tissues of various origins and their efficiency of joining. Here, we report that lungs possess maximum NHEJ activity among the organs, comparable to that in germ cells. Besides, genomic rearrangement proficient thymus and spleen also showed significant joining. However, terminally differentiated tissues present in the organs like kidney, liver and heart showed lower NHEJ. Although joining efficiency varied among organs, the mode of joining was generally comparable.

Materials and methods

Enzymes, chemicals and reagents

Chemical reagents were obtained from Sigma Chemical (St. Louis, MO, USA), Amresco (USA) and Sisco Research Laboratories (India). DNA modifying enzymes were from New England Biolabs (Beverly, MA, USA) and antibodies were purchased from Santa Cruz Biotechnology (USA). Radioisotope-labeled nucleotides were purchased from BRIT (India).

Oligomers

Oligomers used for the study are listed in Supplementary Table 1. The oligomers were purified using 8–12% denaturing PAGE and when required complementary oligomers were annealed in 100 mM NaCl and 1 mM EDTA in boiling water bath for 10 min followed by slow cooling as described [47].

5′ end-labeling

The 5′ end-labeling of the oligomeric DNA was performed as described [48], using T4 polynucleotide kinase in a buffer containing 20 mM Tris–acetate (pH 7.9), 10 mM magnesium acetate, 50 mM potassium acetate, 1 mM DTT and [γ-^{32}P]ATP at 37°C for 1 h. The labeled substrates were purified using Sephadex G-50 column and stored at −20°C.

Preparation of DNA substrates

The oligomeric DNA substrate containing 5′ overhangs (compatible ends) was prepared by annealing [γ-^{32}P] ATP end-labeled 75 nt oligomer, TSK1 with unlabeled 75 nt complementary oligomer, TSK2. Similarly, substrates containing 5′–5′ noncompatible overhangs and 5′–3′ noncompatible overhangs were prepared by mixing [γ-^{32}P] ATP end labeled, TSK1 with unlabeled complementary oligomers, VK11 and VK13, respectively (Suppl. Fig. 1A). Blunt ended substrates were prepared by annealing [γ-^{32}P] ATP labeled 75 mer, VK7 with unlabeled 75 mer, VK8.

Preparation of cell-free extracts

Cell-free extracts were prepared in ice cold conditions as described [43]. In brief, brain (B), testis (T), thymus (Th), spleen (S), lungs (L), heart (H), liver (Lv) and kidney (K) were collected from male Wistar rats, *Rattus norvegicus* (4–6 weeks old). After washing with ice-cold PBS, tissues were minced to prepare single cell suspensions. They were washed 3–4 times with ice-cold PBS to remove blood and other debris. Testicular cells were then counted using a haemocytometer and equivalent packed cell volume (PCV) was used for other tissues. Approximately, 2×10^7 cells/ml were pelleted (1,200*g*, 10 min), resuspended in hypotonic buffer (buffer A: 10 mM Tris–HCl (pH 8.0), 1 mM EDTA, 5 mM DTT and 0.5 mM PMSF), and homogenized with protease inhibitors (1 μg/ml each of leupeptin, aprotinin, chymostatin and pepstatin). An equal volume of buffer B (50 mM Tris–HCl (pH 8.0), 10 mM $MgCl_2$, 2 mM DTT, 0.5 mM PMSF, 25% sucrose and 50% glycerol) was added which was followed by addition of neutralized, saturated ammonium sulfate solution (11% cut off) with stirring (30 min). Then supernatant was collected after centrifugation (3 h at 32,000*g* at 2°C). Proteins precipitated by ammonium sulfate (65%) were pelleted, dissolved in dialysis buffer (buffer C: 25 mM HEPES–KOH (pH 7.9), 0.1 M KCl, 12 mM $MgCl_2$, 1 mM EDTA, 2 mM DTT and 17% glycerol) and dialyzed for 16 h. Clarified extracts were aliquoted, quick-frozen in liquid nitrogen and stored at −80°C until use. Protein concentration (6–10 mg/ml) was determined by Bradford's method. The protein amount was further normalized with respect to that of rat testicular extract by loading on SDS-PAGE followed by Coomassie brilliant blue (CBB) and silver staining (Suppl. Fig. 1B-D).

NHEJ assay

NHEJ assay was performed by incubating 4 nM of radiolabeled oligomeric DNA with 2 μg of extracts in a buffer consisting of 30 mM HEPES–KOH (pH 7.9), 7.5 mM $MgCl_2$, 1 mM DTT, 2 mM ATP, 50 μM dNTPs and 0.1 μg BSA in a reaction volume of 10 μl (Suppl. Fig. 1) at 30°C for testes, which is its physiological temperature and 37°C for other tissues. The incubation time was 2 h for compatible ends while it was 6 h for blunt and noncompatible termini. NHEJ reactions were terminated by addition of EDTA (10 mM) and proteinase K. The products were purified by phenol/chloroform extraction, followed by precipitation with ethanol and glycogen, and pellet was dissolved in 10 μl of TE. The reaction products were resolved on 8% denaturing PAGE. The gel was dried, exposed, and signal was detected using PhosphorImager (FLA9000; Fuji, Japan) and analyzed. Each extract was prepared atleast 3 times and each experiment described was done a minimum of three independent times with very good agreement and used for quantification.

NHEJ assay was also performed on different DNA substrates using immunodepleted extracts (see below) or in presence of DNA-PKcs inhibitor, LY294002 (50 μM) as described [34]. After addition of LY294002 to extracts, the mixture was incubated for 30 min on ice, shifted to 37°C (for testis 30°C) for 15 min, to which substrate was added and incubated for 6 h.

For quantification of joined products, Multi Guage (V3.0) software was used. A rectangle covering the DNA band in one lane was selected and its intensity was quantified. The same sized rectangle was then placed over the substrate band and other joined product bands, and quantified in each lane. An equal area from the same lane of the gel, where there was no specific band, was used as background and was subtracted from each. Band intensities of the products were then added from each lane. The % joining efficiency was calculated using the equation (intensity of total joined products × 100)/(intensity of average of remaining substrates + joined products) and represented as photo-stimulated luminescence (PSL)/mm^2 for each lane. Finally, the efficiency of joining between tissues was compared by plotting a bar diagram and statistical analysis was done using GraphPad Prism (V5) software.

The overall joining efficiency of each tissue was calculated by averaging the joining efficiency of all four DSBs studied. Since testis showed the highest joining efficiency among all tissues studied, it was considered as 100%. The efficiency of joining for other tissues was calculated relative to that of testis (Table 1).

Table 1 Comparison of NHEJ efficiency in different somatic tissues with respect to testicular cells

Tissue	Relative NHEJ efficiency (%)
Brain	43.33
Testis	100
Thymus	50.54
Spleen	49.67
Lungs	82.96
Heart	1.703
Liver	12.26
Kidney	16.52

Efficiency of NHEJ was calculated independently for 5′ overhang, blunt, 5′–5′ noncompatible and 5′–3′ noncompatible ends. The data shown are the relative average efficiency calculated for all four substrates by considering the efficiency of testis as 100

T7 exonuclease assay

The purified NHEJ reaction products were incubated with 2.5 and 7.5 U of T7 exonuclease in a buffer containing 2 mM Tris-acetate (pH 7.9), 1 mM magnesium acetate, 5 mM potassium acetate and 100 μM DTT at 25°C for 2 h. The final products were resolved on 8% denaturing PAGE and visualized as described above.

PCR amplification, cloning and sequencing of NHEJ junctions

The NHEJ products were cut out from PAGE after acquiring the image and DNA was eluted using TE and NaCl (500 mM). The purified DNA was used for PCR amplification of NHEJ junctions using VK24 and SS37 primers. Gel purified PCR products were ligated with TA vector and used for transformation of *E. coli*. Junctions from the clones of interest were then purified and sequenced (Macrogen, South Korea).

Immunodepletion of NHEJ proteins

Immunoprecipitation of NHEJ proteins were performed as described [49]. Approximately, 40 μg of rat testicular extracts were incubated with 4 μl of antibody (0.2 μg/μl) against LIGASE IV, KU70 and KU80 (14 h, at 4°C). The mixture was incubated with Protein G agarose beads for 4 h, beads were spun down to collect the supernatant (immunodepleted fraction), which was then used for NHEJ assay. For western blotting, whole cell and immunodepleted extracts were electrophoresed on a SDS-PAGE, transferred onto a PVDF membrane and probed with antibodies against KU70, KU80 and LIGASE IV (see below). To determine the efficiency of immunodepletion, the intensity of bands obtained before and after immunodepletion were quantified and presented as a bar diagram.

Semi-quantitative PCR

Rat tissues of interest were collected, snap-frozen in liquid nitrogen and used for RNA extraction using Trizol (TRI Reagent; Sigma) as per manufacturer's instructions. DNase (Fermentas) treatment was given to all the RNA samples and the cDNA was prepared using M-MuLV Reverse Transcriptase (Fermentas) (1 h at 37°C) using oligo $(dT)_{18}$. For each sample, a reaction without reverse transcriptase was also done. The amount of cDNA was normalized for Gapdh and used for PCR. Amplifications were performed using appropriate primers for Ku70, Ku80, Artemis, Ligase IV and Xrcc4, and products were resolved on agarose gel (1%).

Immunoblotting

For immunoblotting analysis, ~60 μg protein was resolved on 8–10% SDS-PAGE. Following this, proteins were transferred to PVDF membrane (Millipore, USA), blocked with 5% skimmed milk powder for 1–2 h at room temperature, probed with appropriate primary antibodies against rat KU70 (1:750), KU80 (1:750), DNA-PKcs (1:500), XRCC4 (1:750), LIGASE IV (1:750), POLλ (1:750), GAPDH (1:1,000), ARTEMIS (1:500), p53 (1:750) and BRCA1 (1:200). The numbers in the parenthesis indicate the dilution. Blots were washed in PBST (1× PBS and 0.1% Tween 20) several times and incubated with biotinylated secondary antibodies (Santa Cruz; 1:10,000) at room temperature for 1 h. The blots were rinsed, incubated with 250 ng/ml streptavidin-HRP (Sigma) for 30 min and washed. The blots were developed using chemiluminescent solution (Immobilon™ western; Millipore, USA) and scanned by gel documentation system (LAS 3000; Fuji, Japan). Each western blot has been done a minimum of three independent times and bands were quantified as described above.

Purification of XRCC4 and joining assay

XRCC4 was cloned into pET28a and expressed in *E. coli* BL21(DE3)pLysS as described [50]. Briefly, overnight grown culture was inoculated into LB media, induced at mid-log phase with 1 mM IPTG and allowed to grow for 2 h at 37°C. The cells were pelleted and protein was extracted in 20 mM Tris–HCl (pH 8.0), 0.5 M KCl, 20 mM imidazole (pH 7.0), 20 mM 2-mercaptoethanol, 10% glycerol, 0.2% Tween-20, 1 mM PMSF and 0.1 mg/ml lysozyme. The lysate was then clarified by centrifugation (30,000*g*, 1 h) and loaded onto a Ni-NTA column (Novagen). Following washing, the protein was eluted at ~200 mM imidazole and collected as multiple fractions. The presence and purity of XRCC4 in the fractions were checked on a SDS-PAGE. Peak fractions were pooled and dialyzed against buffer (20 mM Tris–HCl (pH 8.0), 150 mM KCl, 2 mM DTT and 10% glycerol). The presence of XRCC4 was further confirmed by western blotting using XRCC4 antibody. For NHEJ assay, ~500 ng of XRCC4 was added to the rat heart extract and incubated with DNA substrates (5′ compatible and 5′–5′ non-compatible termini). In the case of control, equivalent volume of dialysis buffer was added to the extracts and incubated with substrate DNA. After purification, DNA was loaded onto 8% denaturing PAGE.

Immunofluorescence staining

Histological sections were prepared from brain, testis, thymus, spleen, lung, heart, liver and kidney of 4- to 6-week-old rats as per standard protocols. After dewaxing in xylene and rehydration in graded alcohols, the sections were boiled in 10 mM citrate buffer and preincubated with blocking buffer (20% horse serum, 1% BSA and 0.1% Tween 20). Tissue sections were incubated with anti-KU70 (1:100) or anti-LIGASE IV (1:50) antibody followed by incubation with biotinylated universal secondary antibody (Vectorshield; 1:500) and addition of streptavidin-FITC. The sections were counterstained with 4,6-diamidino-2-phenylindole (DAPI), rinsed, dehydrated and mounted with anti-fade mounting medium. Sections were observed under a fluorescence microscope (Nikon, Japan) at a magnification of ×40 and documented.

Results

Efficiency of NHEJ varies among somatic tissues

Earlier, we have shown an efficient NHEJ in mouse testicular cells [43, 44]. However, there are no studies to compare the efficiency and mechanism of NHEJ among germ and somatic cells. We have used an oligomer-based cell-free assay system to study NHEJ in different tissues of rat. The different steps involved in the NHEJ assay and four different substrates used for assaying NHEJ are outlined (Suppl. Fig. 1A). Briefly, [γ-^{32}P]ATP end labeled 75-bp double-stranded oligonucleotide containing different ends was incubated with cell-free extracts for 2 or 6 h, purified and resolved on a denaturing PAGE. To compare efficiency of NHEJ in different somatic tissues and testis, cell-free extracts were prepared from brain, thymus, spleen, lung, heart, liver and kidney of rats and protein concentration was normalized with that of testis using Bradford's estimation and gel assay (Suppl. Fig. 1B-D and data not shown). The protein titration (1, 2, 5, 10 μg) and time kinetics indicated that 0.2 μg/μl, and 2 h of incubation was optimal for efficient joining, when DNA substrates with 5′ compatible ends were used (Suppl. Fig. 2 and data not shown). Boiled extracts did not catalyze any joining, indicating that the protein components are required for the end-joining and is specific to the extracts (data not shown).

In order to compare the DSB repair efficiencies between somatic and testicular cells, we used substrates mimicking different types of endogenous DSBs. First, we incubated radiolabeled oligomeric DNA substrate containing 5′ overhangs (Suppl. Fig. 1) with 2 μg each of cell-free extracts. Results showed that the extracts catalyzed efficient end-joining resulting in dimers, trimers, and other forms of multimers in the case of brain, testis, spleen, lungs and kidney (Fig. 1a, lanes 2, 3, 5, 6, and 9). In addition to these products, additional bands were also visible between substrate and dimer band, which were confirmed as circular products (see below). In the case of thymus, kidney and liver, the compatible end-joining was weak, while heart showed much lower level of joining (Fig. 1b). When blunt end substrates were used for NHEJ assay, maximum joining was observed in testis and lungs, while thymus and spleen showed moderate joining (Fig. 1c). Brain, heart, liver and kidney showed lower joining as compared to their activity on 5′ overhang substrates (Fig. 1b, c). NHEJ assay with 5′–5′ and 5′–3′ noncompatible ends showed that overall joining efficiency was lower in comparison to compatible ends (Fig. 1b, d, e). In these cases also, testis and lungs showed maximum repair efficiency (Fig. 1d, e). In the case of 5′–5′ overhangs, brain, thymus and spleen showed moderate joining (Fig. 1d). In the case of 5′–3′ noncompatible substrates, thymus showed efficient joining similar to that of lungs (Fig. 1e), while spleen and brain showed moderate joining. Interestingly, liver, kidney and heart exhibited lowest joining efficiency in the case of both noncompatible ends (Fig. 1d, e). Thus, based on different DSBs studied, we conclude that the overall efficiency of NHEJ varied between testicular cells and somatic cells derived from different organs. Among somatic tissues, lungs showed highest NHEJ activity (Table 1). Thymus, spleen and brain showed significant joining, while activity was poor or undetectable in the case of kidney, liver and heart (Table 1).

We observed distinct additional bands between DNA substrates and 150 bp dimer products (Fig. 1a). To identify the nature of these bands, T7 exonuclease, an enzyme that acts in 5′–3′ direction on linear DNA, but not on circular DNA, was used. End-joined products from rat testicular extracts were treated with T7 exonuclease and resolved on denaturing PAGE. Results showed that T7 exonuclease was able to digest the bands corresponding to monomeric substrate and linear dimer DNA, but not the bands in between (Fig. 1f). The presence of the uncleaved products suggested their circular nature.

NHEJ in cell-free extracts of rat tissues follow different mode of joining

In order to study sequence characteristics of end-joined junctions, they were PCR amplified, cloned and sequenced (Suppl. Fig. 3). In the case of 5′ compatible and blunt end substrates, we digested the obtained clones with *Bam*HI and *Sma*I, since a simple ligation without end processing would recreate the *Bam*HI and *Sma*I site, respectively. We found that all the analyzed clones were recleavable indicating that there were no modifications at the junctions

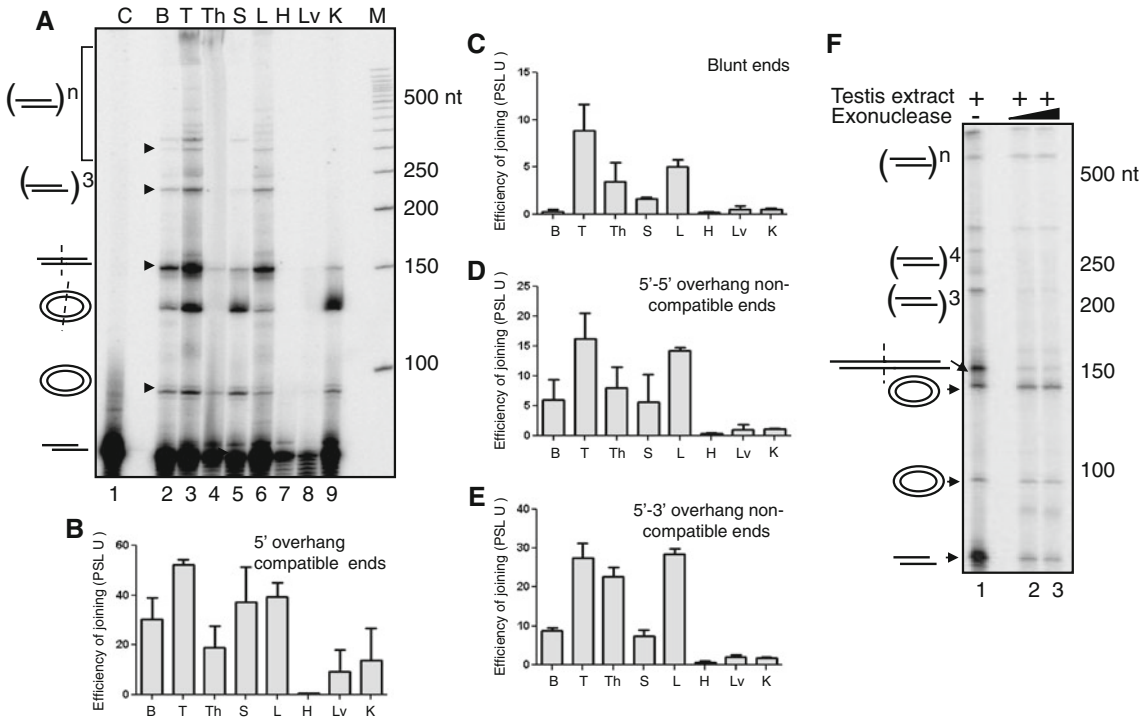

Fig. 1 Comparison of efficiency of endjoining catalysed by different rat tissues upon incubation with DNA substrates possessing different DSBs. Approximately 2 μg of protein was incubated (2 h) with 4 nM of [γ-^{32}P] ATP labeled DNA substrate (75-mer) in NHEJ buffer and products were purified and resolved on a denaturing PAGE. **a** NHEJ assay on DSBs containing 5′ overhangs. **b** *Bar diagram* showing quantification of NHEJ products derived from DSBs with 5′ overhang. **c** *Bar diagram* showing quantification of NHEJ products from blunt end DNA substrates. **d** *Bar diagram* showing quantification of NHEJ products derived from DSBs with 5′–5′ noncompatible ends. **e** *Bar diagram* showing quantification of NHEJ products derived from DSBs with 5′–3′ noncompatible ends. In **c**–**e**, incubation time for NHEJ reactions was 6 h. In all panels, tissues studied are, brain (*B*), testis (*T*), thymus (*Th*), spleen (*S*), lungs (*L*), heart (*H*), liver (*Lv*), and kidney (*K*). The efficiency of the joining is quantified and presented as PSL units. Data from three independent experiments are used for quantification and *error bars* (SEM, $p < 0.05$) are indicated. In **a**, *lane 1*, substrate alone (*C*) *M* is radiolabeled 50 bp ladder. **f** T7 exonuclease assay to identify conformation of NHEJ products. The end joined products (*lane 1*) were treated with 2.5 (*lane 2*) and 7.5 U (*lane 3*) of T7 exonuclease (25°C for 2 h) and products were resolved on denaturing PAGE. Molecular weights are indicated

obtained from these substrates (data not shown). Sequences of the NHEJ junctions from each tissue were categorized as M1, M2, M3 and M4 based on characteristic features for both 5′–5′ and 5′–3′ noncompatible termini (Figs. 2, 3). Results showed that, in the case of brain, among the 15 NHEJ junctions sequenced, the majority joined by no or limited modifications. All 8 junctions derived from 5′–5′ noncompatible termini had 4-nt deletion of the overhang from one end and end-filling at the other overhang (Fig. 2a, M1). In one of the clones, an insertion at the junction and a 2-nt deletion in an arm was also observed (Fig. 2a). In the case of NHEJ junction resulting from 5′–3′ ends, 2/7 clones had deletions from both sides (Fig. 2b, M2). Other clones were joined by ligation of single-strand overhang followed by template dependent synthesis (Fig. 2b, M4).

In the case of testis, among the 37 NHEJ junctions sequenced, only 3 molecules had longer deletions while the other 34 had minimum modifications at the junctions (Fig. 2). In 5′–5′ NHEJ junctions, all 20 junctions sequenced had AATT overhang deletion from one end, while in 17 cases other ends joined by end-filling and ligation (Fig. 2a, M1). Among these, three molecules had extensive deletions and joined using 1 nt microhomology (Fig. 2a, M3). In the case of 5′–3′ overhang substrates, single-strand ligation of overhangs followed by DNA synthesis and ligation was observed in all 17 junctions (Fig. 2b, M4). In thymus, 5′–5′ noncompatible end joining followed standard mechanism in which one overhang was deleted, while the second one was end-filled before ligation (Fig. 2a, M1). In addition, three molecules had longer deletions of which two had a “T” insertion (Fig. 2a, M2). In the case of 5′–3′ noncompatible junctions, we noted that two NHEJ junctions utilized 3- and 5-nt microhomology during the end-joining (Fig. 2b, M3). In one of the clones, 2-nt duplication was also observed (Fig. 2b).

Spleen did not show much modification at NHEJ junctions of both 5′–5′ and 5′–3′ termini (Fig. 2a, M1; b, M4). In the case of lungs, a total of 28 NHEJ junctions were sequenced andthe results showed that the joining mechanism was similar to that in testis. In 13/15 junctions derived

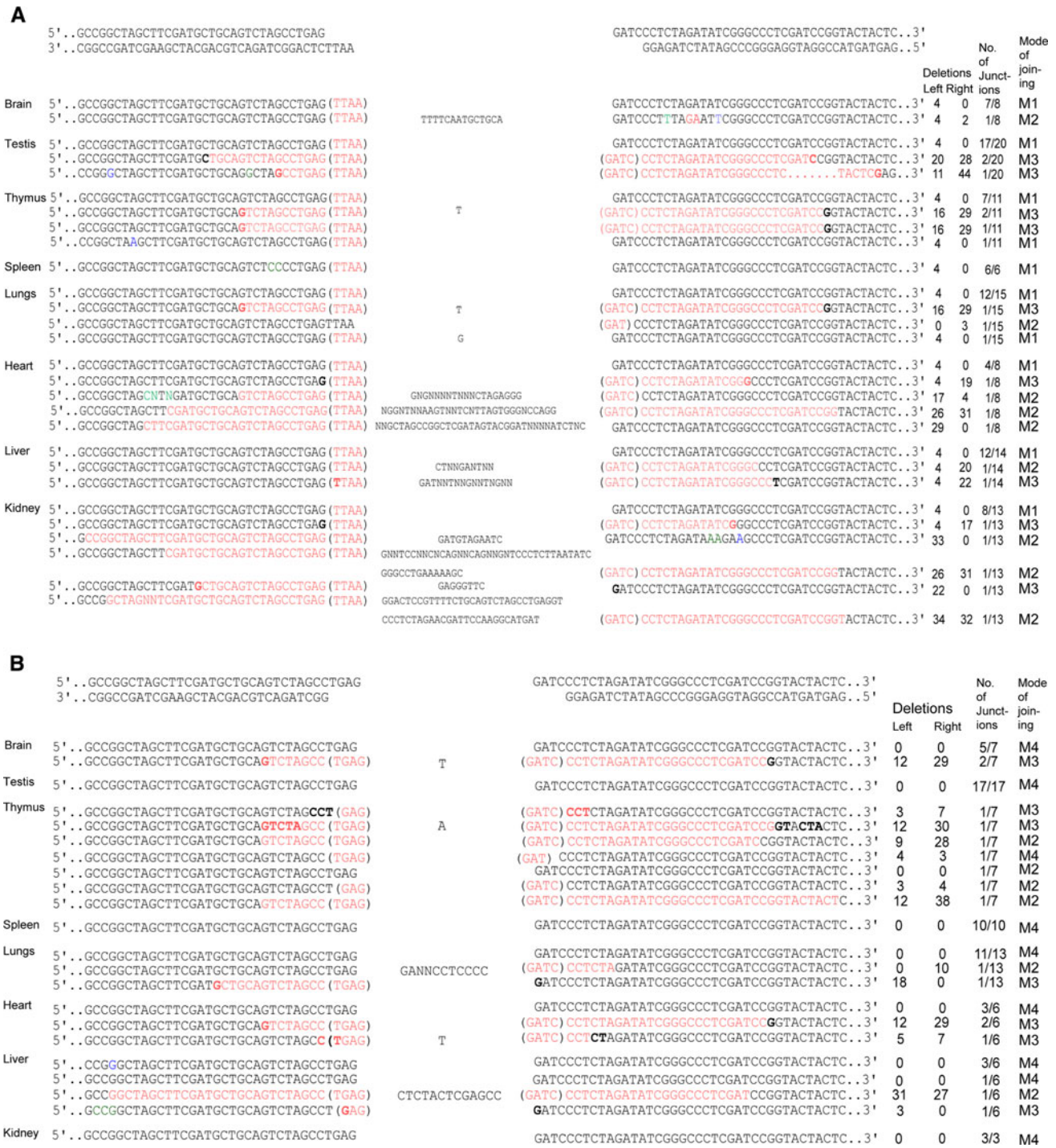

Fig. 2 Sequence analysis of NHEJ junctions. Joined products of noncomplementary ends (5′–5′ or 5′–3′) were eluted from the gel, purified, PCR amplified and ligated in TA vector. Clones of interest were screened by restriction enzyme digestion and used for sequencing. Sequences were aligned based on substrates and tissues. **a** Features of NHEJ junctions derived from 5′–5′ noncompatible ends. **b** Sequence characteristics of NHEJ junctions derived from 5′–3′ noncompatible ends. The sequences denoted in red color are the nucleotides deleted. The nucleotides deleted from the overhang are indicated in *brackets*. The nucleotides in the *middle column* indicate the sequences inserted at the junctions. Single nucleotide insertion (*blue*) and point mutation (*green*) are also indicated. Nucleotides indicated in bold are the microhomology sequences. Four major modes of joining based on sequence analysis have been depicted as *M1*, *M2*, *M3* and *M4* (refer to Fig. 7 for more details). *M1* indicates NHEJ junction due to removal of an overhang, followed by end-filling of the other and ligation. *M2* indicates that both the overhangs were deleted, and resulting ends were ligated. *M3* refers to the microhomology mediated joining. *M4* refers to single-strand ligation of overhangs followed by DNA synthesis and ligation

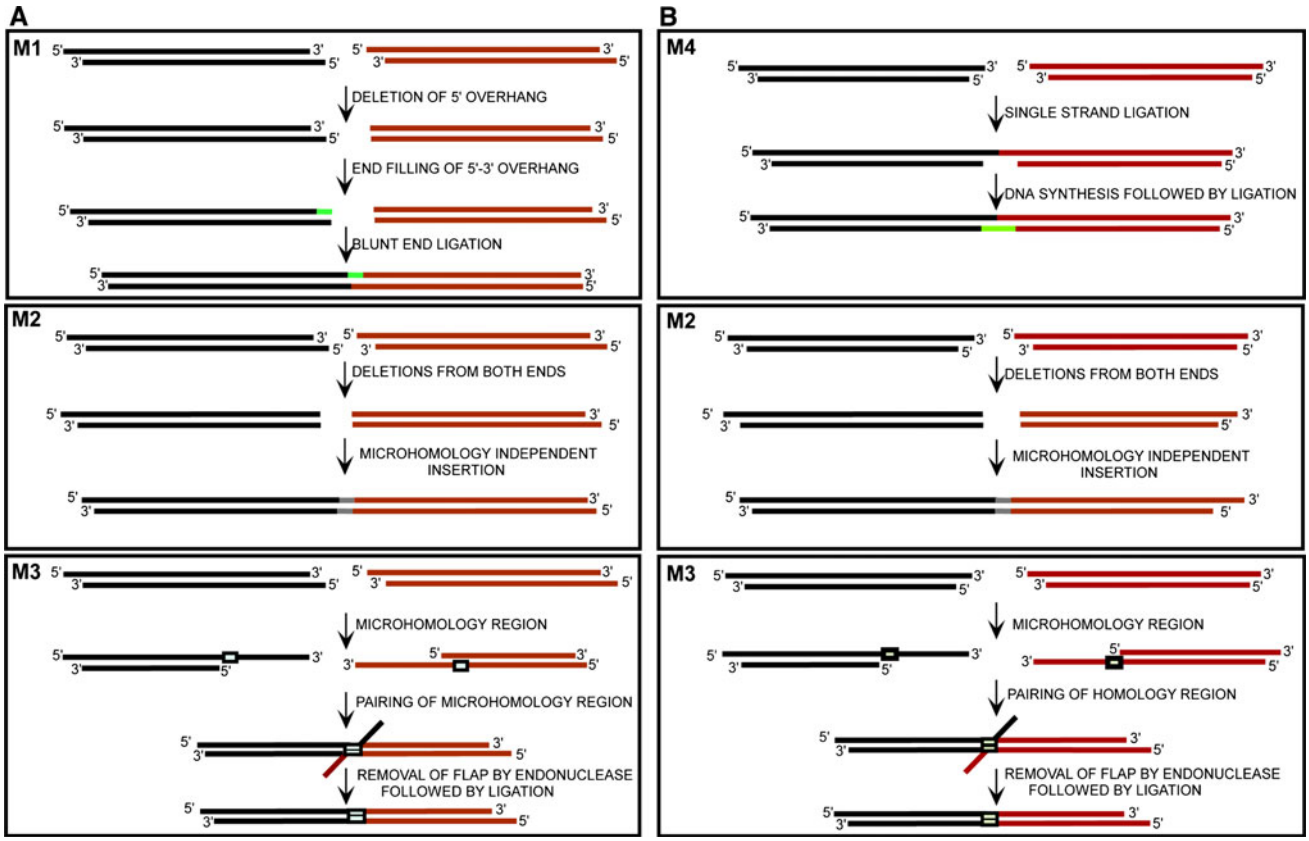

Fig. 3 Proposed mechanism of NHEJ in rat tissues. **a** In the case of 5′–5′ noncompatible ends, three different mechanisms are proposed. In the first mechanism, one of the 5′ overhangs is deleted and the second overhang is filled and then ligated. In the second mechanism, both the 5′ overhangs are deleted and then ligated. In third mechanism, the two ends are joined using microhomology. A stretch of nucleotides are deleted from both the overhangs till microhomology region is exposed. Then the two ends are ligated. **b** In the case of 5′–3′ overhangs, two mechanisms are proposed. In the first, both overhangs are ligated resulting in single-strand break joining followed by fill-in by DNA polymerase. Second mechanism is mediated by microhomology as depicted in **a**. In both the panels, two independent substrate molecules are shown using two different colors (*maroon* and *blue*). Each double-stranded DNA molecule is represented as *double lines* with *overhangs*. The newly synthesized regions are indicated, and microhomology regions are indicated by a *box*

from 5′–5′ noncompatible ends, joining was by deletion of AATT overhang, followed by end-filling of the other and ligation (Fig. 2a, M1). The other two clones joined with various length deletions (Fig. 2a, M2, M3). In the case of junctions from 5′–3′ overhang substrates, 11/13 molecules followed the standard mechanism described for testis (Fig. 2b, M4). The other two junctions showed deletion from one end each (Fig. 2b, M2, M3).

Sequencing of NHEJ junctions from heart tissue showed that NHEJ mechanism differed from that of other tissues with 6/14 junctions sequenced having longer deletions (20 bp or more) (Fig. 2, M2, M3), among which three molecules had insertions of 15 nt or more (Fig. 2, M2). This suggested that NHEJ in heart was associated with larger modifications. In the case of liver, NHEJ junctions derived from 5′–5′ overhangs (12/14 cases) involved deletion of 5′ overhang followed by end-filling of the other end and ligation (Fig. 2a, M1). Two clones had extended deletion and insertions (Fig. 2a, M2). In the case of 5′–3′ overhangs, joining also occurred mostly using the standard mechanism (Fig. 2b, M4). Furthermore, 5/13 NHEJ junctions of 5′–5′ overhang had deletions of 17 bp or more in the case of kidney (Fig. 2a, M2). Among these, four had large insertions at the junctions. The 5′–3′ overhangs joined by single-strand ligation of overhangs followed by gap-filling (Fig. 2b, M4). Thus, analysis of junctional sequences from rat tissues suggested that the mode of joining is comparable in tissues with higher NHEJ efficiency, where processing of ends was limited. In contrast, the tissues with lower NHEJ efficiencies showed extensive alterations at the junctions.

Immunodepletion of LIGASE IV and KU proteins, and inhibition of DNA-PKcs affect the end-joining

The observed sequence characteristics of the joined junctions indicate that the joining catalyzed by different extracts occurs through NHEJ. To further test such a

possibility, the major NHEJ proteins (LIGASE IV, KU70 and KU80) were immunoprecipitated and used for end-joining assay. Testicular and lung extracts were selected for immunodepletion studies as these showed maximum efficiency for the NHEJ. When LIGASE IV-depleted extracts were used for the assay, a significant reduction in NHEJ was observed in the case of compatible, noncompatible and blunt end substrates (Fig. 4a and Suppl. Fig. 4A, B). Immunoprecipitation of KU70 also led to a dramatic reduction in NHEJ, which is quantitated and presented (Fig. 4b and Suppl. Fig. 4C, D). However, in the case of KU80, the observed reduction was limited in the case of testis compared to lungs (Fig. 4c and Suppl. Fig. 4E, F). The observed difference in NHEJ efficiency upon immunodepletion of KU70 and KU80 in testis was surprising, since they generally exist as a complex. Therefore, we compared the immunodepletion efficiencies of KU70, KU80 and LIGASE IV using western blotting. Results showed that there was indeed a difference in the efficiency of IP between the proteins, thereby explaining the observed difference in NHEJ (Fig. 4d, e). Thus, our data suggest that the joining was mostly dependent on LIGASE IV, KU70 and KU80 indicating the involvement of classical NHEJ. In addition, we also found that, in the case of compatible ends, immunodepletion of LIGASE IV, KU70, and KU80 led to a reduction in the linear multimers, whereas it resulted in an increase in circularization (Fig. 4a, b and Suppl. Fig. 5).

To corroborate our findings, we also used an inhibitor of DNA-PKcs, LY294002, which has been used to study the role of DNA-PKcs in NHEJ [34]. Then, 2 μg of cell-free extracts was pre-incubated with LY294002 (50 μM) and used for NHEJ reaction with 5′–5′ noncompatible termini. Results showed reduced joining in the case of testis, thymus, spleen and lungs compared to control (Fig. 4f). Thus, our data suggest that the rat tissues catalyze joining through the NHEJ pathway.

Expression of NHEJ genes varies among rat tissues

The above studies suggested that the end-to-end joining observed from different tissues is mediated through NHEJ. Therefore, we were interested in testing whether the observed difference in the efficiency of NHEJ between tissues could be attributed to the differential expression of NHEJ genes. Thus, we tested their expression, both at the transcriptional and translational level. Semi-quantitative RT-PCR using primers against Ku70, Ku80, Ligase IV, Artemis and Xrcc4, was performed to study the expression at RNA level (Fig. 5). Gapdh was used as an internal control. Results showed that all the NHEJ genes analyzed were expressed abundantly in testis and lungs when compared to other tissues (Fig. 5, lanes 4, 10). Thymus also showed elevated expression of Ligase IV, Artemis and Xrcc4 compared to other tissues (Fig. 5, lane 6). Interestingly, heart and liver had lowest expression of almost all the NHEJ genes, especially Ligase IV (Fig. 5, lanes 12, 14). We noted that expression of Ku70 and Artemis was detected in most of the tissues compared to other NHEJ genes (Fig. 5).

Since we could find an interesting correlation between expression of NHEJ genes at transcriptional level and efficiency of NHEJ in different tissues, we further checked the expression at translational level by immunoblotting. GAPDH was used as a loading control since it is constitutively expressed in all tissues (Fig. 6a; Suppl. Fig. 1B–D). Results showed that all the NHEJ proteins analysed were present in testis (Fig. 6a, lane 2). Importantly, lungs and thymus also showed detectable expression of most of the NHEJ proteins (Fig. 6a, lanes 5 and 3). We could observe expression of KU70 and ARTEMIS at the protein level in almost all the tissues (Fig. 6a, b). In a previous study, it was reported that KU70 is present in nuclei of all cell types of testis except in early zygotene spermatocytes [51, 52]. Hence, the observed higher expression of KU70 in testis is consistent with the above reports, although we have not performed the study in isolated testicular cells or in nuclear extracts. Expression of LIGASE IV and XRCC4 was found to be lowest in spleen which may explain lower efficiency of NHEJ. We also observed expression of key NHEJ proteins in brain except for POLλ, where the expression was very low. Surprisingly, expression of many NHEJ proteins was high in liver and kidney, in spite of very low activity. This interesting observation is being investigated currently. In the case of heart, most of the key NHEJ proteins were highly expressed except for XRCC4 (Fig. 6a). We also observed slight differences in the molecular weight of XRCC4 indicating possible isoforms in different tissues. p53 is a tumour suppressor gene involved in activation of DNA repair or apoptosis depending on the extent of DSBs. The expression of p53 was highest in testis and lungs while it was low in spleen, heart, liver and kidney. It was also expressed at a lower level in brain and spleen (Fig. 6a, b). A recent study suggesting regulation of NHEJ by BRCA1 [53] prompted us to test its expression level in different tissues. Results showed that expression of BRCA1 was highest in heart. Its expression was also seen in kidney, liver and testis, while it was undetectable in other tissues (Fig. 6a, b).

We have observed lowest efficiency of NHEJ in heart, despite the presence of all the NHEJ proteins (except XRCC4). Therefore, we wondered whether expression of XRCC4, a stimulating factor for LIGASE IV, plays a critical role in regulating the NHEJ in heart. In order to test the hypothesis, we performed NHEJ assay following addition of purified recombinant XRCC4 protein to the

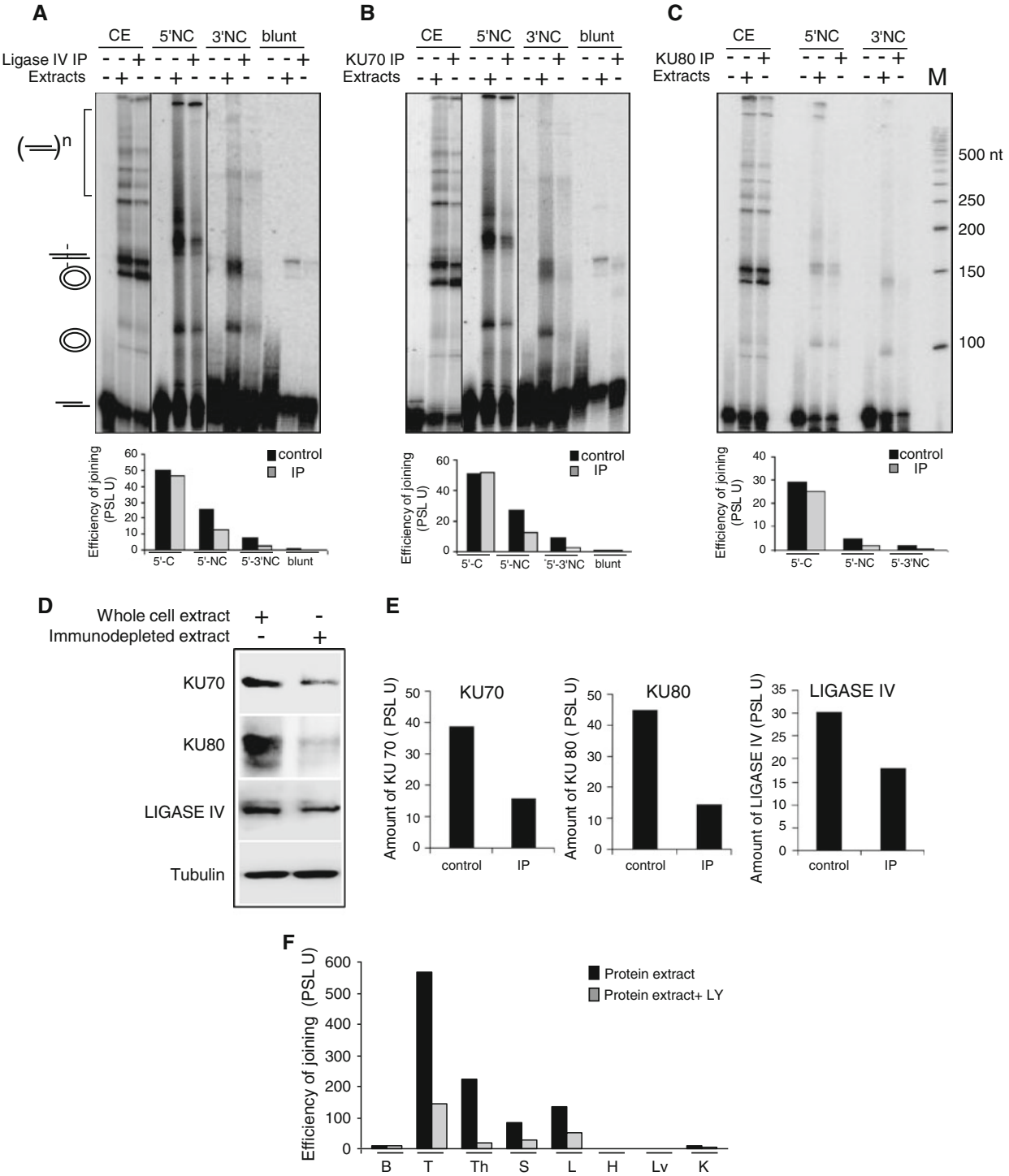

Fig. 4 NHEJ assay following immunodepletion of DNA LIGASE IV, KU70, or KU80 and incubation with DNA-PKcs inhibitor. DNA LIGASE IV (**a**), KU70 (**b**) and KU80 (**c**) proteins were immunoprecipitated using respective antibodies from rat testicular cell extracts using protein-G agarose. Then, NHEJ reactions were carried out with substrates containing different DSBs. Products were resolved on a denaturing PAGE. *CE* 5′–5′ compatible ends, *5′NC* 5′–5′ noncompatible ends, *3′NC* 5′–3′ noncompatible ends and *blunt* for blunt ends. *M* is radiolabeled 50-bp ladder. Joined products of each lane were quantified and presented as a *bar diagram* below respective panels. **d** Western blot analysis of KU70, KU80 and LIGASE IV following immunodepletion of the respective proteins. Tubulin is used as an internal loading control. **e** *Bar diagram* showing comparison of amount of proteins quantified from (**d**). **f** LY294002, a DNA-PKcs inhibitor (50 μM) was incubated with cell-free extracts (2 μg) of brain, testis, thymus, spleen, lungs, heart, liver and kidney along with 5′–5′ noncompatible overhang substrates and the NHEJ products were analyzed as described above and products were quantified and presented as a *bar diagram*

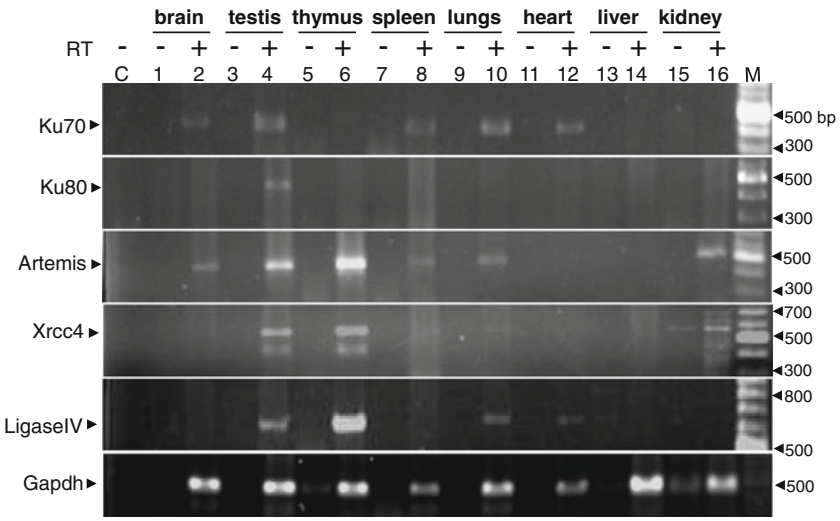

Fig. 5 Semi-quantitative RT-PCR for NHEJ genes in various rat tissues. RNA was extracted from rat tissues, cDNA was synthesized, and used for PCR amplification of NHEJ genes (Ku70, Ku80, Artemis, Ligase IV and Xrcc4). Gapdh was used as an internal control to normalize for cDNA concentrations. Bands of interest are indicated. *M* Molecular weight ladder

heart cell-free extract (Fig. 6c). Interestingly, we found that although addition of XRCC4 improved the efficiency of NHEJ in heart, it was still much lower when compared to other tissues (Fig. 6d, e).

To further confirm the above observations inside cells, we selected two key NHEJ proteins, LIGASE IV and KU70, for immunostaining studies. Histological sections of brain, testis, thymus, spleen, lungs, heart and kidney were stained with appropriate antibodies. The results showed that the expression level of KU70 was similar in all the tissues analyzed, which was consistent with its expression, both at transcriptional and translational levels (Fig. 7a). On the other hand, the expression of LIGASE IV varied among tissues and was higher in testis, thymus, lungs, kidney and brain while it was lower in heart and spleen (Fig. 7b). Hence, the expression of DNA repair proteins may play a vital role in regulating NHEJ machinery in both germ and somatic tissues.

Discussion

DSBs can occur naturally by normal physiological and metabolic processes at a significant frequency. Besides, exogenous factors also contribute to generation of DSBs in different cells of an organism. Thus, DSB repair machinery including NHEJ is active throughout the lifespan of a cell, so that the integrity of the genome is restored to ensure the survival of a cell. Previously, using a plasmid based cell-free repair assay system, efficient NHEJ-mediated DSB repair was reported in mice testis [43, 44]. NHEJ has also been extensively studied in *Xenopus* oocytes [54–57]. Transformed monkey kidney cells have been used for transfection studies to demonstrate NHEJ inside the cells [33, 58]. Studies from somatic cells were based on cell extracts prepared from various cell lines [29, 31, 34, 59–61]. Although these studies have compared the efficiencies of NHEJ, most of them were performed in isolation. Moreover, since cell lines are derived by transforming somatic cells, they may not represent a physiological scenario [41]. In addition, although a cell line is developed from a particular cell of an organ, it might not necessarily behave the same [39–42].

Lung extracts possess highest NHEJ while heart, liver and kidney showed lowest activity

The comparison of NHEJ efficiency between different tissues showed that, similar to testicular cells, lungs also possessed an efficient NHEJ system. The NHEJ efficiency of lungs was greater than any other somatic cells studied (Table 1; Fig. 1). However, sequence analysis of NHEJ junctions suggested that there was no major difference in the mode of joining between lungs, testes, spleen and brain.

Thymus also showed an efficient NHEJ, which is expected as these cells are proficient in V(D)J recombination, the process by which T-cell receptor (TCR) diversity is generated [62]. It is well established that NHEJ seals the cleaved V, D or J ends during final phase of V(D)J recombination [1]. Sequence analysis of junctions from thymus showed extensive alterations in almost every molecule studied (Fig. 2), as thymus possesses many enzymes capable of bringing additional junctional diversity during TCR rearrangement. Earlier studies have also reported efficient NHEJ in calf thymus [63]. Similarly, the observed NHEJ in spleen matches with its properties, as it is a lymphoid organ, harboring B-cells, which undergo class switch recombination [64]. Previous studies using brain cells have also demonstrated an efficient NHEJ using a plasmid-based system, which is consistent with our results [46].

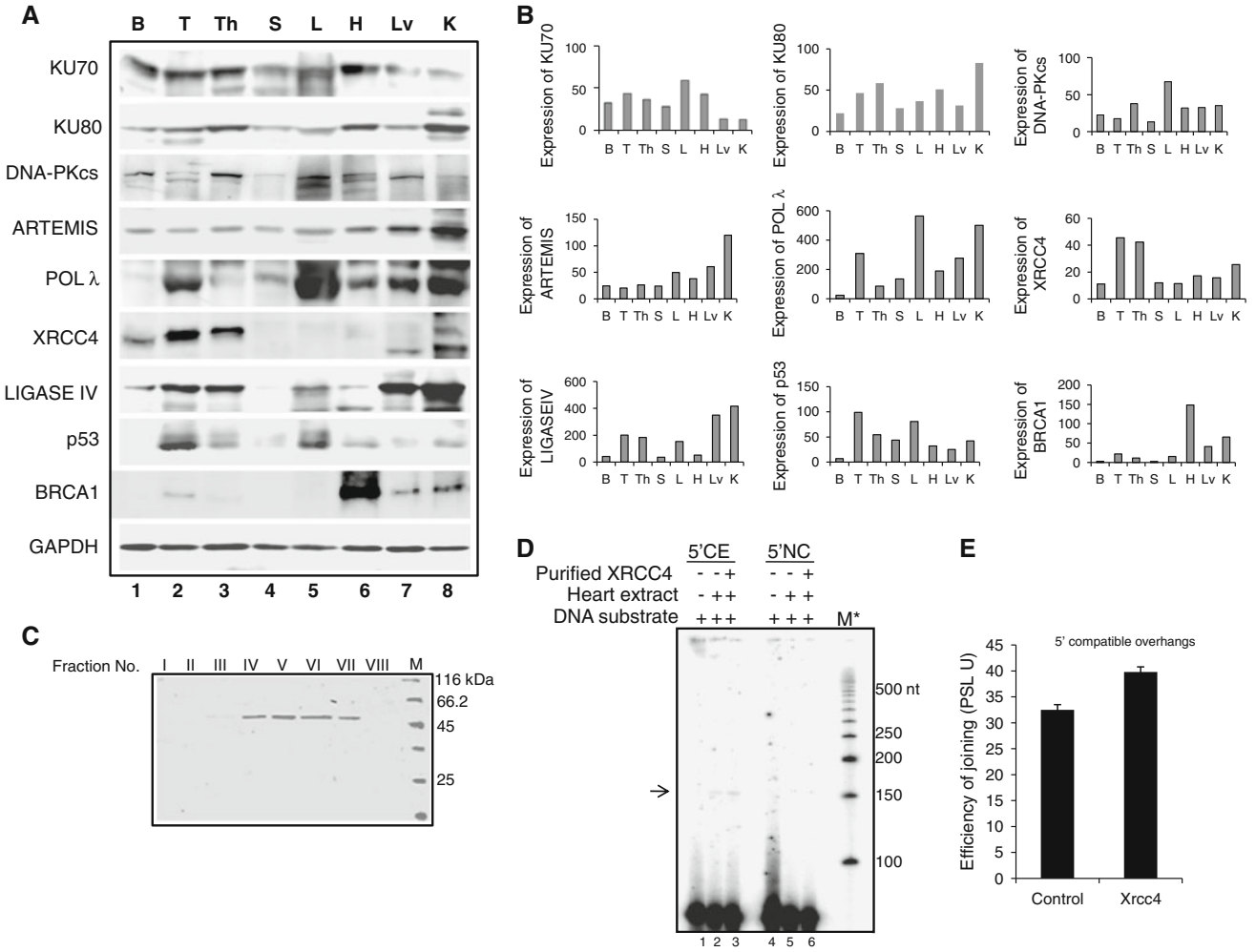

Fig. 6 Western blotting showing expression of repair proteins in rat tissues. Cell-free extracts were prepared from brain (*B*), testis (*T*), thymus (*Th*), spleen (*S*), lungs (*L*), heart (*H*), liver (*Lv*) and kidney (*K*) and resolved on SDS-PAGE. **a** Western blot analysis. 60 μg of extract proteins from rat tissues were resolved on a SDS-PAGE and transferred to PVDF membrane. Appropriate antibodies were used against DSB repair proteins to study the expression of KU70, KU80, DNA-PKcs, ARTEMIS, POL*λ*, XRCC4, LIGASE IV, p53 and BRCA1. **b** Comparison of expression of proteins quantified from the respective blot is shown as *bar diagrams*. **c** SDS-PAGE profile of purified XRCC4 protein. Bacterial cell lysate containing overexpressed XRCC4 was loaded on to a Ni-NTA column and the fractions were collected. The purified protein was resolved on a PAGE and stained with CBB. The image shown is in *gray scale*. *M* Molecular weight ladder for proteins. **d** NHEJ assay on DSBs containing 5′ overhangs with compatible and non-compatible termini using rat heart extracts following addition of purified XRCC4. *Lanes 1*, *4* DNA substrate; *lanes 2*, *5* substrate incubated with heart extract and equivalent volume of dialysis buffer; *lanes 3*, *6* substrate incubated with heart extract and purified XRCC4 protein. *M** Radiolabeled 50-bp ladder. **e** *Bar diagram* showing quantification of NHEJ products obtained from 5′ compatible ends from (**d**)

Among the tissues studied, heart, kidney and liver exhibited lowest NHEJ activity. This is surprising based on the observation that kidney, heart and liver have efficient expression of most of the NHEJ proteins. Since the cells in these organs do not divide actively, it could be possible that the cells with DSBs may be more easily tolerated. We also wondered whether such a contradiction is due to presence of some inhibitory factors, characteristic of certain cell types with respect to joining, as these organs contain mostly terminally differentiated cells. Very recently, we noted that separation of proteins by fractionation of kidney extracts led to an elevated joining efficiency compared to whole cell extracts (T.S.K. and S.C.R., unpublished data). This is one reason which makes cell-free extracts a difficult system for analysis of NHEJ. This may be due to factors such as nuclear/cytoplasmic ratio, which may determine how much 'contamination' occurs with other proteins relative to the level of NHEJ proteins. Nevertheless, there is merit and value in knowing the overall level of apparent NHEJ activity in crude extracts. This indicates that, although joining efficiency can be correlated with expression of NHEJ genes, in the cases of kidney, liver and heart,

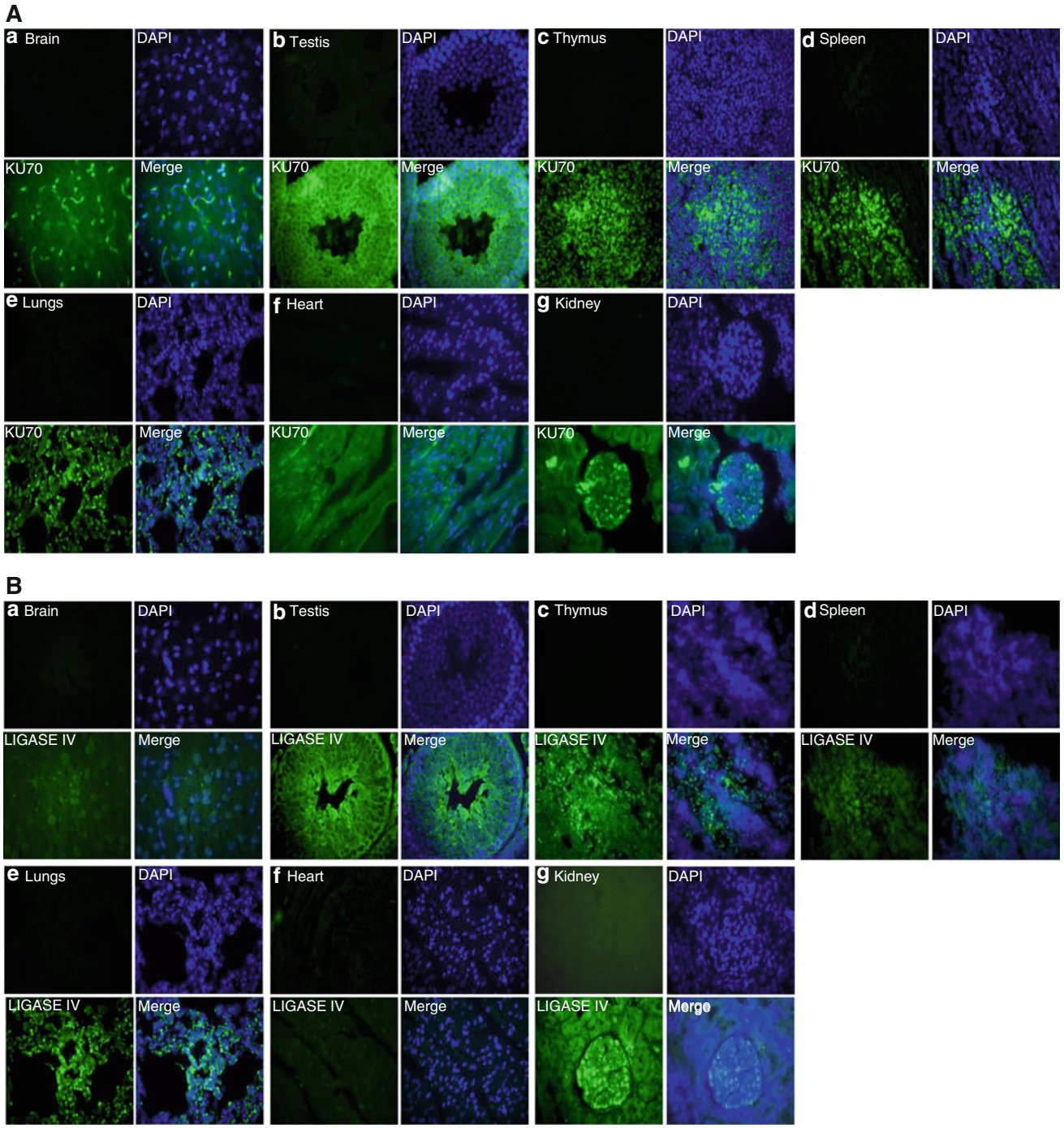

Fig. 7 Localization of KU70 and LIGASE IV by immunostaining in various rat tissues. Immunofluoroscence for KU70 (**a**) and LIGASE IV (**b**) were carried out using respective anti-KU70 and anti-LIGASE IV and FITC-conjugated secondary antibody (*green*) and nuclear stain DAPI (*blue*). Images were taken at a magnification of ×40. Tissues used are **a** brain, **b** testis, **c** thymus, **d** spleen, **e** lungs, **f** heart, and **g** kidney. In each panel, *upper left* is secondary antibody alone (control), *upper right* panel is stained with DAPI, *lower left* panel of each set is positive immunostaining using FITC alone, while *lower right* is the merged image. Liver tissue could not be analyzed due to its high auto fluorescence

NHEJ may be regulated at other levels, which needs to be explored further.

In the case of heart, it is important to point out that there is a major protein species at ∼150 kDa that makes up a large percentage of the total extracts (Suppl. Fig. 1B, C). It is unclear whether this protein has any role in regulating NHEJ, and this is being investigated. Nevertheless, it is apparent that other proteins including the ones for NHEJ

would be proportionally lower in a specified quantity of total protein cell extract due to the presence of the above protein. In fact, this may contribute towards lower efficiency of NHEJ in heart.

Inositol hexakisphosphate (IP6) has also been shown to regulate NHEJ [65]. It could be possible that IP6 levels vary between different tissues resulting in the observed difference in efficiency of NHEJ. However, this needs to be studied.

Mode of joining differs between tissues

Sequence analysis of NHEJ junctions of 5′–5′ noncompatible termini revealed three independent modes for repair. Deletion of one overhang, followed by end-filling of the second and ligation was the predominant mechanism in all the tissues (Figs. 3a, M1 and 2a). In the second case, both the overhangs were deleted independently, and the resulting ends were ligated (Fig. 3a, M2). In the third mechanism, 1- to 2-nt microhomology region was exposed by exonuclease action, alignment followed by processing of the flap region, possibly by ARTEMIS and then ligation (Fig. 3a, M3). Three independent mechanisms were also observed for 5′–3′ noncompatible termini junctions. In most tissues, single-strand ligation of overhangs followed by gap-filling and ligation was the main mechanism (Figs. 3a, M4 and 2a). The second mechanism involves deletion of ends from both termini followed by joining (Fig. 3b, M2). The third mechanism utilizes microhomology as described (Fig. 3b, M3). It has been shown that microhomology-mediated end joining uses DNA LIGASE I and III, but not DNA LIGASE IV [66]. Since the length of the microhomology region in the present study is mostly 1–2 bp, it needs to be studied further whether the observed microhomology-mediated joining is LIGASE I/III dependent. Another study had previously demonstrated microhomology-mediated end joining in the case of nuclear extracts derived from rat testis [67]. Generally, at least two independent modes of mechanism operate for each terminus examined for a particular tissue in our study.

Why would lungs possess better NHEJ efficiency among somatic tissues?

Genomic insults acquired by lungs due to xenotoxic stress are very high compared to other somatic tissues. Alveoli of lungs are continuously exposed to oxygen, which itself could be a source of DNA damage due to oxidative stress [68]. In contrast to other somatic tissues, cells of lungs are consistently exposed to different pollutants in the air, which could induce DNA breaks. The constant exposure to such mutagens would have helped lungs to evolve with an efficient NHEJ system to repair DSBs.

The above hypothesis is further supported by the observed elevated level of cancers related to lungs. Lung cancer accounts for approximately 30% of all cancer-related deaths. It is reported that lung cancer patients have a lower DNA repair capacity in comparison to healthy individuals [69]. In fact, non-small cell lung cancer (NSCLC) has been associated with genomic instability, which was due to polymorphism in DSB repair genes emphasizing an active DSB repair machinery in lungs [70]. In a different study, it was also shown that suppression of KU70 increases radio- and chemosensitivity in human lung carcinoma cell lines [71]. Microsatellite genotyping study indicated that polymorphism in DSB repair genes can modulate lung cancer susceptibility and prognosis [72]. However, we do not find such an elevated NHEJ in the case of liver, which is also exposed to a variety of xenotoxic agents. As discussed above, this could be due to some other factors regulating NHEJ, which is being investigated.

LIGASE IV dependent classical NHEJ is predominant in rat tissues

Immunodepletion and inhibitor studies showed the involvement of KU proteins, LIGASE IV and DNA-PKcs, during NHEJ activity. These proteins are involved in recognizing the ends, recruiting other proteins and ligation of broken ends [8, 10, 14]. Hence, our results show that the observed joining is LIGASE IV- and KU70-dependent indicating dominance of classical NHEJ. Previously, it has been shown that KU is very important for joining, since it serves as an alignment factor for bringing the two DNA ends together, in addition to its role in protecting the ends of DSBs and thus increasing both the efficiency and accuracy of NHEJ [17, 73–75]. Consistent with this observation, in our studies, we find that most of the DNA sequences of the joined junctions were preserved with limited alterations, especially in tissues in which the joining was efficient. We also noted that, generally, when joining was low, there were more molecules with extensive deletions. Hence, our study opens a new window for correlation of the NHEJ pathway in various somatic tissues and their genomic rearrangements due to endogenous and exogenous damages, which could help in understanding the mechanism of radiosensitivity and thereby oncogenesis.

Acknowledgments We would like to thank Dr. Kumaravel Somasundaram, IISc for providing us with the BRCA1 antibody. We thank Dr. Kavitha C.V. for her help in western blot experiments. We also thank Dr. Binu Tharakan, Abhishek K.V., Mrinal Srivastava, Mridula Nambiar, Nishana M. and other members of SCR laboratory for discussions and help. This work was supported by grant from DAE, India (2008/37/5/BRNS) and IISc start up grant for SCR. We also thank Dr. Raghavan Varadarajan for financial assistance. SS acknowledges Senior Research Fellowship from DBT, India.

Conflict of interest Authors disclose that there is no conflict of interest.

References

1. Lieber MR, Yu K, Raghavan SC (2006) Roles of nonhomologous DNA end joining, V(D)J recombination, and class switch recombination in chromosomal translocations. DNA Repair (Amst) 5:1234–1245
2. Ferguson DO, Alt FW (2001) DNA double strand break repair and chromosomal translocation: lessons from animal models. Oncogene 20:5572–5579
3. Khanna KK, Jackson SP (2001) DNA double-strand breaks: signaling, repair and the cancer connection. Nat Genet 27:247–254
4. Nambiar M, Kari V, Raghavan SC (2008) Chromosomal translocations in cancer. Biochim Biophys Acta 1786:139–152
5. Lieber MR (2008) The mechanism of human nonhomologous DNA end joining. J Biol Chem 283:1–5
6. Weterings E, Chen DJ (2008) The endless tale of non-homologous end-joining. Cell Res 18:114–124
7. Burma S, Chen BP, Chen DJ (2006) Role of non-homologous end joining (NHEJ) in maintaining genomic integrity. DNA Repair (Amst) 5:1042–1048
8. Wyman C, Kanaar R (2006) DNA double-strand break repair: all's well that ends well. Annu Rev Genet 40:363–383
9. Jackson SP (2002) Sensing and repairing DNA double-strand breaks. Carcinogenesis 23:687–696
10. Hefferin ML, Tomkinson AE (2005) Mechanism of DNA double-strand break repair by non-homologous end joining. DNA Repair (Amst) 4:639–648
11. Lieber MR, Ma Y, Pannicke U, Schwarz K (2003) Mechanism and regulation of human non-homologous DNA end-joining. Nat Rev Mol Cell Biol 4:712–720
12. Sonoda E, Sasaki MS, Buerstedde JM, Bezzubova O, Shinohara A, Ogawa H, Takata M, Yamaguchi-Iwai Y, Takeda S (1998) Rad51-deficient vertebrate cells accumulate chromosomal breaks prior to cell death. EMBO J 17:598–608
13. Takata M, Sasaki MS, Sonoda E, Morrison C, Hashimoto M, Utsumi H, Yamaguchi-Iwai Y, Shinohara A (1998) Homologous recombination and non-homologous end-joining pathways of DNA double-strand break repair have overlapping roles in the maintenance of chromosomal integrity in vertebrate cells. EMBO J 17:5497–5508
14. Lieber MR, Lu H, Gu J, Schwarz K (2008) Flexibility in the order of action and in the enzymology of the nuclease, polymerases, and ligase of vertebrate non-homologous DNA end joining: relevance to cancer, aging, and the immune system. Cell Res 18:125–133
15. Yano K, Morotomi-Yano K, Adachi N, Akiyama H (2009) Molecular mechanism of protein assembly on DNA double-strand breaks in the non-homologous end-joining pathway. J Radiat Res (Tokyo) 50:97–108
16. Chiruvella KK, Sankaran SK, Singh M, Nambiar M, Raghavan SC (2007) Mechanism of DNA double-strand break repair. ICFAI J Biotech 1:7–22
17. Mimori T, Hardin JA (1986) Mechanism of interaction between Ku protein and DNA. J Biol Chem 261:10375–10379
18. Falzon M, Fewell JW, Kuff EL (1993) EBP-80, a transcription factor closely resembling the human autoantigen Ku, recognizes single- to double-strand transitions in DNA. J Biol Chem 268: 10546–10552
19. West RB, Yaneva M, Lieber MR (1998) Productive and non-productive complexes of Ku and DNA-dependent protein kinase at DNA termini. Mol Cell Biol 18:5908–5920
20. Ma Y, Pannicke U, Schwarz K, Lieber MR (2002) Hairpin opening and overhang processing by an Artemis/DNA-dependent protein kinase complex in nonhomologous end joining and V(D)J recombination. Cell 108:781–794
21. Ma Y, Lu H, Tippin B, Goodman MF, Shimazaki N, Koiwai O, Hsieh CL, Schwarz K, Lieber MR (2004) A biochemically defined system for mammalian nonhomologous DNA end joining. Mol Cell 16:701–713
22. Nick McElhinny SA, Ramsden DA (2004) Sibling rivalry: competition between Pol X family members in V(D)J recombination and general double strand break repair. Immunol Rev 200:156–164
23. Tseng HM, Tomkinson AE (2002) A physical and functional interaction between yeast Pol4 and Dnl4-Lif1 links DNA synthesis and ligation in nonhomologous end joining. J Biol Chem 277:45630–45637
24. Mahajan KN, Nick McElhinny SA, Mitchell BS, Ramsden DA (2002) Association of DNA polymerase mu (pol mu) with Ku and ligase IV: role for pol mu in end-joining double-strand break repair. Mol Cell Biol 22:5194–5202
25. Grawunder U, Wilm M, Wu X, Kulesza P, Wilson TE, Mann M, Lieber MR (1997) Activity of DNA ligase IV stimulated by complex formation with XRCC4 protein in mammalian cells. Nature 388:492–495
26. Wilson TE, Grawunder U, Lieber MR (1997) Yeast DNA ligase IV mediates non-homologous DNA end joining. Nature 388:495–498
27. Ahnesorg P, Smith P, Jackson SP (2006) XLF interacts with the XRCC4-DNA ligase IV complex to promote DNA nonhomologous end-joining. Cell 124:301–313
28. Labhart P (1999) Nonhomologous DNA end joining in cell-free systems. Eur J Biochem 265:849–861
29. North P, Ganesh A, Thacker J (1990) The rejoining of double-strand breaks in DNA by human cell extracts. Nucleic Acids Res 18:6205–6210
30. Sankaranarayanan K, Wassom JS (2005) Ionizing radiation and genetic risks XIV. Potential research directions in the post-genome era based on knowledge of repair of radiation-induced DNA double-strand breaks in mammalian somatic cells and the origin of deletions associated with human genomic disorders. Mutat Res 578:333–370
31. Budman J, Chu G (2005) Processing of DNA for nonhomologous end-joining by cell-free extract. EMBO J 24:849–860
32. Roth DB, Wilson JH (1985) Relative rates of homologous and nonhomologous recombination in transfected DNA. Proc Natl Acad Sci USA 82:3355–3359
33. Roth DB, Wilson JH (1986) Nonhomologous recombination in mammalian cells: role for short sequence homologies in the joining reaction. Mol Cell Biol 6:4295–4304
34. Baumann P, West SC (1998) DNA end-joining catalyzed by human cell-free extracts. Proc Natl Acad Sci USA 95:14066–14070
35. Jones HW Jr, McKusick VA, Harper PS, Wuu KD (1971) George Otto Gey. (1899–1970). The HeLa cell and a reappraisal of its origin. Obstet Gynecol 38:945–949
36. Giard DJ, Aaronson SA, Todaro GJ, Arnstein P, Kersey JH, Dosik H, Parks WP (1973) In vitro cultivation of human tumors: establishment of cell lines derived from a series of solid tumors. J Natl Cancer Inst 51:1417–1423
37. Foley GE, Lazarus H, Farber S, Uzman BG, Boone BA, McCarthy RE (1965) Continuous culture of human lymphoblasts from peripheral blood of a child with acute leukemia. Cancer 18:522–529

38. Raju MR, Trujillo TT, Mullaney PF, Romero A, Steinkamp JA, Walters RA (1974) The distribution in the cell cycle of normal cells and of irradiated tumour cells in mice. Br J Radiol 47:405–410
39. Short SC, Martindale C, Bourne S, Brand G, Woodcock M, Johnston P (2007) DNA repair after irradiation in glioma cells and normal human astrocytes. Neuro Oncol 9:404–411
40. Barret JM, Calsou P, Larsen AK, Salles B (1994) A cisplatin-resistant murine leukemia cell line exhibits increased topoisomerase II activity. Mol Pharmacol 46:431–436
41. Cai QQ, Plet A, Imbert J, Lafage-Pochitaloff M, Cerdan C, Blanchard JM (1994) Chromosomal location and expression of the genes coding for Ku p70 and p80 in human cell lines and normal tissues. Cytogenet Cell Genet 65:221–227
42. Sandberg R, Ernberg I (2005) Assessment of tumor characteristic gene expression in cell lines using a tissue similarity index (TSI). Proc Natl Acad Sci USA 102:2052–2057
43. Sathees CR, Raman MJ (1999) Mouse testicular extracts process DNA double-strand breaks efficiently by DNA end-to-end joining. Mutat Res 433:1–13
44. Raghavan SC, Raman MJ (2004) Nonhomologous end joining of complementary and noncomplementary DNA termini in mouse testicular extracts. DNA Repair (Amst) 3:1297–1310
45. Vyjayanti VN, Rao KS (2006) DNA double strand break repair in brain: reduced NHEJ activity in aging rat neurons. Neurosci Lett 393:18–22
46. Ren K, Pena de Ortiz S (2002) Non-homologous DNA end joining in the mature rat brain. J Neurochem 80:949–959
47. Naik AK, Raghavan SC (2008) P1 nuclease cleavage is dependent on length of the mismatches in DNA. DNA Repair (Amst) 7:1384–1391
48. Naik AK, Lieber MR, Raghavan SC (2010) Cytosines, but not purines, determine recombination activating gene (RAG)-induced breaks on heteroduplex DNA structures: implications for genomic instability. J Biol Chem 285:7587–7597
49. Milne GT, Jin S, Shannon KB, Weaver DT (1996) Mutations in two Ku homologs define a DNA end-joining repair pathway in *Saccharomyces cerevisiae*. Mol Cell Biol 16:4189–4198
50. Modesti M, Hesse JE, Gellert M (1999) DNA binding of Xrcc4 protein is associated with V(D)J recombination but not with stimulation of DNA ligase IV activity. EMBO J 18:2008–2018
51. Goedecke W, Eijpe M, Offenberg HH, van Aalderen M, Heyting C (1999) Mre11 and Ku70 interact in somatic cells, but are differentially expressed in early meiosis. Nat Genet 23:194–198
52. Hamer G, Roepers-Gajadien HL, van Duyn-Goedhart A, Gademan IS, Kal HB, van Buul PP, Ashley T, de Rooij DG (2003) Function of DNA-protein kinase catalytic subunit during the early meiotic prophase without Ku70 and Ku86. Biol Reprod 68:717–721
53. Zhong Q, Boyer TG, Chen PL, Lee WH (2002) Deficient nonhomologous end-joining activity in cell-free extracts from Brca1-null fibroblasts. Cancer Res 62:3966–3970
54. Daza P, Reichenberger S, Gottlich B, Hagmann M, Feldmann E, Pfeiffer P (1996) Mechanisms of nonhomologous DNA end-joining in frogs, mice and men. Biol Chem 377:775–786
55. Pfeiffer P, Gottlich B, Reichenberger S, Feldmann E, Daza P, Ward JF, Milligan JR, Mullenders LH, Natarajan AT (1996) DNA lesions and repair. Mutat Res 366:69–80
56. Lehman CW, Clemens M, Worthylake DK, Trautman JK, Carroll D (1993) Homologous and illegitimate recombination in developing Xenopus oocytes and eggs. Mol Cell Biol 13:6897–6906
57. Pont-Kingdon G, Dawson RJ, Carroll D (1993) Intermediates in extrachromosomal homologous recombination in *Xenopus laevis* oocytes: characterization by electron microscopy. EMBO J 12:23–34
58. Roth DB, Porter TN, Wilson JH (1985) Mechanisms of nonhomologous recombination in mammalian cells. Mol Cell Biol 5:2599–2607
59. Thacker J, Chalk J, Ganesh A, North P (1992) A mechanism for deletion formation in DNA by human cell extracts: the involvement of short sequence repeats. Nucleic Acids Res 20:6183–6188
60. Fairman MP, Johnson AP, Thacker J (1992) Multiple components are involved in the efficient joining of double stranded DNA breaks in human cell extracts. Nucleic Acids Res 20:4145–4152
61. Nicolas AL, Young CS (1994) Characterization of DNA end joining in a mammalian cell nuclear extract: junction formation is accompanied by nucleotide loss, which is limited and uniform but not site specific. Mol Cell Biol 14:170–180
62. Kindt TJ, Goldsby RA, Osborne BA (2007) Kuby immunology. Freeman, New York
63. Mason RM, Thacker J, Fairman MP (1996) The joining of non-complementary DNA double-strand breaks by mammalian extracts. Nucleic Acids Res 24:4946–4953
64. Honjo T, Alt FW, Neuberger M (2004) Molecular biology of B cells. Elsevier, London
65. Hanakahi LA, Bartlet-Jones M, Chappell C, Pappin D, West SC (2000) Binding of inositol phosphate to DNA-PK and stimulation of double-strand break repair. Cell 102:721–729
66. Liang L, Deng L, Nguyen SC, Zhao X, Maulion CD, Shao C, Tischfield JA (2008) Human DNA ligases I and III, but not ligase IV, are required for microhomology-mediated end joining of DNA double-strand breaks. Nucleic Acids Res 36:3297–3310
67. Boan F, Blanco MG, Barros P, Gomez-Marquez J (2006) DNA end-joining driven by microhomologies catalyzed by nuclear extracts. Biol Chem 387:263–267
68. Karanjawala ZE, Murphy N, Hinton DR, Hsieh C-L, Lieber MR (2002) Oxygen metabolism causes chromosome breaks and is associated with the neuronal apoptosis observed in double-strand break repair mutants. Curr Biol 12:397–402
69. Shen H, Spitz MR, Qiao Y, Guo Z, Wang LE, Bosken CH, Amos CI, Wei Q (2003) Smoking, DNA repair capacity and risk of nonsmall cell lung cancer. Int J Cancer 107:84–88
70. Zienolddiny S, Campa D, Lind H, Ryberg D, Skaug V, Stangeland L, Phillips DH, Canzian F, Haugen A (2006) Polymorphisms of DNA repair genes and risk of non-small cell lung cancer. Carcinogenesis 27:560–567
71. Omori S, Takiguchi Y, Suda A, Sugimoto T, Miyazawa H, Tanabe N, Tatsumi K, Kimura H, Pardington PE, Chen F, Chen DJ, Kuriyama T (2002) Suppression of a DNA double-strand break repair gene, Ku70, increases radio- and chemosensitivity in a human lung carcinoma cell line. DNA Repair (Amst) 1:299–310
72. Tseng RC, Hsieh FJ, Shih CM, Hsu HS, Chen CY, Wang YC (2009) Lung cancer susceptibility and prognosis associated with polymorphisms in the nonhomologous end-joining pathway genes: a multiple genotype–phenotype study. Cancer 115:2939–2948
73. Feldmann E, Schmiemann V, Goedecke W, Reichenberger S, Pfeiffer P (2000) DNA double-strand break repair in cell-free extracts from Ku80-deficient cells: implications for Ku serving as an alignment factor in non-homologous DNA end joining. Nucleic Acids Res 28:2585–2596
74. Ramsden DA, Gellert M (1998) Ku protein stimulates DNA end joining by mammalian DNA ligases: a direct role for Ku in repair of DNA double-strand breaks. EMBO J 17:609–614
75. Lee SE, Moore JK, Holmes A, Umezu K, Kolodner RD, Haber JE (1998) Saccharomyces Ku70, mre11/rad50 and RPA proteins regulate adaptation to G2/M arrest after DNA damage. Cell 94:399–409